ELECTRON BEAM WRITING AND DIRECT PROCESSING SYSTEM FOR NANOLITHOGRAPHY

H. Hiroshima, S. Okayama, M. Ogura, M. Komuro,

*H. Nakazawa, *Y. Nakagawa, *K. Ohi, and *K. Tanaka

Electrotechnical Laboratory 1-1-4 Umezono, Tsukuba, Ibaraki, 305 JAPAN

*JEOL LTD. 1-2 Musashino, 3-chome Akishima, Tokyo, 196 JAPAN

This article describes the electron beam direct processing system developed for patterning beyond the resolution limit of conventional resists by using inorganic resists or electron beam induced surface reactions. A probe beam with the probe current of 120 pA was focused into 3nm with the newly developed optical column. An ultra high vacuum sample chamber, which can coexist with a precise stage driving mechanism and a LASER measuring system, was constructed by adapting a double chamber stage system. The base pressure of the sample chamber after baking was $1x10^{-8}$ Torr and differential evacuation of the sample chamber and the mechanism chamber was demonstrated. The stabilities of the stage and the optical column were measured with a LASER measuring system and mark detection procedures. The standard deviations of stitching and overlay accuracy measured by an exposure of PMMA were 20nm and 40nm, respectively. An exposure of PMMA resists revealed that this EB system can delineated the lines with the ultimate resolution of PMMA resists.

1. Introduction

For developing electronic devices based on quantum effects, shrinkage of dimension of devices is the key to demonstrate the functions. Electron beam (EB) direct writers which can delineate 10-20nm wide pattern onto organic resists[1], is thought to be one of the most promising tools for nanofabrications. However, demands of such devices are exceeding the resolution limit of conventional organic resists. Inorganic resists such as metal-oxides and -halides are candidates of higher resolution resists[2, 3]. Contamination resist[4] which is a kind of EB induced surface reaction may also be a candidate. If the vacuum quality around the sample is excellent and appropriate gases are introduced, direct etching of target materials and deposition of metals can be carried out by EB induced surface reactions[5, 6]. In addition, these techniques have an advantage of positioning, since an image or a position of the target is obtained by scanning the probe beam. It is possible that the minimum fabrication size is defined by the size of the probe beam. Those processes must be carried out in an ultra high vacuum (UHV), otherwise contaminations grown by the EB irradiation degrade the patterning resolution and prevent the aimed EB induced reactions[3]. The sizes of samples and patterns and the available process were restricted far from device fabrication because no precise positioning system has been installed in a UHV system. In case that conventional EB direct writers are applied to the above processes, reducing the base pressure into a UHV range is difficult by baking the stage mechanism and the position measuring system with keeping their precisions. We tried to solve the above problem by

adapting a double chamber stage system[7] to the newly developed EB writing and direct processing system as shown in Fig. 1.

2. System concept

2. 1 Electron optics

Figure 2 shows the ray diagram of the electron optics. A ZrO/W thermal field emitter[8] of which the characteristics is an excellent brightness and a triplet lens system with a zooming function are adapted. The higher beam voltage is preferable in order to reduce the aberration of diffraction and the broadening in the target by a forward scattering. We select the acceleration voltage of 50 kV, considering the reliability of a high voltage system. The Gun lens (lens 1) is an Orloff-Swanson type electrostatic lens[9] of which the aberration coefficients are low. The others are electromagnetic lenses. The total spherical (Cs) and chromatic (Cc) aberration coefficients are written as follows[10]:

$$Cs = Cs_1 \cdot (M_2 \cdot M_3)^4 + Cs_2 \cdot M_3^4 + Cs_3 \qquad (1)$$

$$Cc = Cc_1 \cdot (M_2 \cdot M_3)^2 + Cc_2 \cdot M_3^2 + Cc_3 \qquad (2)$$

where all of coefficients are referred to the image side. The basic strategy of fine focusing is that the lens 3 operates at a low magnification and that aberration coefficients of the lens 3 are reduced. An objective lens with low aberration coefficients is designed and the working distance is minimized as small as possible. The optical path is also shortened as small as possible. The working distance and the optical path are 16mm and 381 mm, respectively. The optical parameters of lenses at a typical operating condition are summarized

in Table 1. The zooming action of lens 1 and lens 2 varies the probe current with keeping second focal plane at the center of blanking electrodes. The probe diameters as a function of the probe current for given aperture sizes are calculated in Fig. 3 using a measured angular current density of 0.4 mA/sr at 3.6 kV and assuming the source size and the energy spread of emitted electrons of 30 nm and 1 eV[8], respectively, where the total magnification varies from 0.006 to 0.11. The calculation predicts that the probe size of 2.5 nm is available for the probe current of 100pA for the aperture diameter of 60 μm corresponding the convergent half angle of 3.74 mrad.

2.2. Ultra high vacuum sample chamber

A schematic view of the developed double chamber stage system is illustrated in Fig. 1. The inner chamber is a sample chamber which includes a part of the stage and the outer is a mechanism chamber which includes mirrors for LASER measuring system, stage guides, bearings and so on. The stage moves with keeping the gap between the moving plate (the hatched part in Fig. 1) and the stationary plate 0.3 mm wide. The calculated conductance of the gap is 0.6 l/s which corresponds to that of an orifice with a diameter of 0.25 mm. As the precise parts of the stage are excluded from the sample chamber, we can bake the sample chamber and expect that the pressure of the sample chamber becomes in UHV range after baking. The gap prevents not only the residual gases in the mechanism chamber from diffusing into the sample chamber but also the process gases in the sample chamber from diffusing into the mechanism chamber in case of EB induced surface

reactions. By adapting a double chamber stage system, we can use reliable stage mechanisms and we need not care their chemical protections.

2. 3. Total system

Figure 4 shows a photograph of the developed EB direct processing system. The probe size is reduced with the optical system mentioned above. A secondary electron detector and backscattered electron detectors are installed in the sample chamber for detection of sample images and mark positions. A retractable gas injection nozzle is attached in the UHV sample chamber, which is adjusted a few tenth mm above the sample in order to make a high gas flux with a small gas flow. By monitoring the status of the nozzle position, a computer restricts the traveling area of the stage in order not to crush the nozzle. The optical column is separated with orifices into some chambers which are evacuated by independent pumps and the sample chamber and the two neighboring chambers are evacuated with chemical proof turbo molecular pumps (TMPs) through vibration dampers. Samples are exchanged through the loading chamber without breaking the vacuum of the sample chamber. Available sample sizes are 2 inch wafer and a 10 mm square wafer. The maximum field size is 80 μm x 80 μm and the EB system has stitching and overlay functions. The exposure sequence is controlled by a computer where data types of JEOL01, JEOL51, PG-3000 and PG-3600 are available. The principal specifications are summarized in Table 2.

3. System performance

The probe diameter was measured by a knife edge method. A Au coated Ni mesh was used as a knife edge and a p-n junction detector was located underneath. By the probe beam scanned over the edge, the current profile of the probe beam was measured. The probe diameter was determined by a scanning distance where the measured current varies from 15% to 85% of the probe current. The typical results are shown in Figs. 5(a) and 5(b), where the probe current was 120 pA and the convergent half angle was 3.74 mrad. The results includes about 10 % errors by vibrations. Though the probe is not stigmatic yet, the result shows that the 3 nm beam with the probe current of 120 pA is available. The measured probe diameters for 3 different convergent half angles are plotted in Fig. 3, where the data represent the minimum value in many trials since the poor edge condition enlarges the measured probe diameter. The experimental results agree with the calculation within 20 % errors. Thus we can conclude that the column operates as designed.

The sample chamber was baked at 150°C with panel heaters surrounding the sample chamber, where the temperature of the stage top raised 40°C. The pressure after baking was $1x10^{-8}$ Torr which was a quarter of that before baking. The base pressure is somewhat higher than what we expected. Figure 6 shows the pressures of the gun chamber and the mechanism chamber in the case of gas introduction. In this experiment, the pressure of the sample chamber was varied by decelerating the TMP evacuating the sample chamber. Note that the pressure of $1x10^{-4}$ Torr corresponds to the gas introduction 10 times as large as the rated maximum gas flow. The estimated conductance of the gap of

the double chamber stage system was a few times larger than the calculation. it seems to be caused by miss adjustment of the gap. However, as two orders of pressure difference was achieved, we think that the stage mechanism will act well in case of EB induced chemical reaction processes. In addition, the electron source will hardly be damaged since the pressure of the gun chamber was not varied at all in this experiment. We think that the base pressure of the UHV sample stage will be improved by baking the portion of the stage in the sample chamber with additional heaters and by adjusting the gap width correctly.

Figure 7 shows the long term stability of the stage. The stage position was measured with the LASER measuring system with an interval of 0.1 sec. The data represent the stage positions averaged for 1 min. The result means not only that the drift of the stage in 25 min is less than 2 nm but also that the drift of the LASER measuring system is less than 2 nm.

The typical short term stability of the stage is shown in Fig. 8(a). In this experiment, the stage position was detected with interval of 500 usec. Vibration with the peak-to-peak value of 5 to 10 nm exists. Figure 8(b) shows the power spectrum of the vibration. The principal peaks with an amplitude of 1 nm are at 100 Hz and 600 Hz. The former is the resonance frequency of the stage and the latter the rotating frequency of TMPs. We expect the vibration at 100 Hz will also be reduced by killing the vibration from the TMP with additional dampers.

The stability of a landing position of the 50 kV EB was measured

by means of mark detection procedures without stage movement, where gold cross lines on Si substrate were used as a mark. The detected mark position varies within 20 nm for 20 min. The gradually change in the detected position may be caused by the drift of the temperature.

A measurement of stitching and overlay accuracy was carried out by exposing 16 test patterns on a PMMA resist. The test pattern was composed of 4x4 fields where the scale patterns as shown in Fig. 10 were distributed on every field boundary. The deviations at the same portion of different chips were evaluated by an SEM inspection. The results of 128 locations are shown in Figs. 11(a)-11(c). the standard deviations of stitching and overlay are 20 nm and 40 nm, respectively. These values are relatively good, however somewhat inferior to the values of standard JEOL JBX-6000FS[11]. As the sample is not in the plane of the LASER beam paths in this EB system (see Fig. 1), a pitching of the stage changes the sample position even if the measured position with the LASER measuring system is not changed. We think that the degradation of precision is caused by such a phenomenon. This may be a disadvantage of this EB system. However, it will not a serious problem for our purpose, because the exposure of the key portion of nanopatterns are probably smaller than the field size of 80 μm in the most cases.

A fine patterning test was carried out on a 30 nm thick PMMA resist spun on a Si wafer. The beam voltage was 50kV and the probe current was 115pA. After exposure, the resist was developed using 1:3 MIBK:IPA at 22°C for 60 sec and coated with Au/Pd before SEM inspections. Figure 12 shows an SEM image of the delineated lines with a

linedoses of 0.67 nC/cm. The 60 nm pitch lines with a width of about 15 nm were delineated. Thus, it can be conclude that the EB system derives the resolution limit from PMMA resists[1].

4. conclusions

The electron writing and direct processing system has been developed, which is compatible with inorganic resist exposure and EB induced surface reaction process. The UHV sample chamber coexists with the precision stage system by using the double chamber stage system. The base pressure of the sample stage is $1x10^{-8}$ Torr and the ability of differential evacuation is demonstrated. The long term stability of the stage is excellent though a small vibration exists. An electron beam with a probe diameter of 3 nm and a probe current of 120 pA is available at a 50kV accelerating voltage. The stitching and overlay accuracy are good but somewhat inferior to those of the state of the art system. It will not be a serious problem for our purpose of nanofabrications. We can conclude that the EB system has an enough potential to develop nanoscale devices.

REFERRENCES

[1] A. N. Broers, J. Electrochem. Soc. 128 (1981) 166.

[2] H. Hiroshima and M. Komuro, Jpn. J. Appl. Phys. 32 (1993) 6153.

[3] I. G. Salisbury, R. S. Timsit, S. D. Berger, and C. J. Humphreys, Appl. Phys. Lett. 45 (1984) 1289.

[4] Y. Ochiai, M. Baba, H. Watanabe, and S. Matsui, Proc. 1991 Int. MicroProcess conf, Kanazawa(Publication Office of Jpn. J. Appl. Phys, Tokyo, 1991) JJAP Series 5, p. 362.

[5] Y. Sugimoto, K. Akita, M. Taneya, and H. Hidaka, Appl. Phys. Lett. 57 (1990) 1012.

[6] S. Matsui and K. Mori, J. Vac. Sci. Technol. B4 (1986) 299.

[7] S. Okayama, M. Ogura, M. Komuro, and H. Hiroshima, Japan Patent 5-90792 (1993); U. S. Patent 8-206161 (1993); German Patent P4408523. 0; Dutch Patent 94. 00393.

[8] L. W. Swanson, Electron Optical Systems (SEM Inc, Chicago, 1984), p. 137.

[9] J. Orloff and L. W. Swanson, J. Appl. Phys. 50 (1979) 2494.

[10] J. Orloff, Optik 63 (1983) 369.

[11] W. B. Thompson, Y. Nakagawa, M. Hasel Shearer, H. Nakazawa, H. Takemura, M. Isobe, and N. Goto, Proc. SPIE vol. 1089 (San Jose, 1989) p. 260.

Table 1. Optical parameters of lenses.

	Lens 1	Lens 2	Lens 3	Total
M	1.2	0.2	0.1	0.024
Cs	16400 mm	127 mm	43.7 mm	43.8 mm
Cc	1820 mm	19 mm	15.2 mm	16.1 mm
Optical path				381 mm
Working distance				16 mm

Table 2. Principal specifications.

Acceleration voltage	50 kV
Cathode	ZrO/W TFE
Probe size and current	3 nm at 100 pA
Scanning step	2.5 nm, 1.25 nm
Field size	80 μm x 80 μm
Stitching accuracy	20 nm(σ)
Overlay accuracy	40 nm(σ)
Substrate size	2 inch, 10 mm□
Base pressure of sample chamber	$\leqq 10^{-8}$ Torr
allowable gas flow	$\leqq 10^{-3}$ Torr l/sec

Fig. 1. Schematic view of the electron beam writing and direct processing system.

Fig. 2. Schematic ray diagram.

Fig. 3. Probe diameter as a function of probe current.

Fig. 4. Photograph of the electron beam writing and direct processing system.

Fig. 5. Probe diameter measured by a knife edge method. (a) X-direction; (b) Y-direction. The acceleration voltage and the probe current are 50 kV and 120 pA, respectively.

Fig. 6. Pressures of the gun chamber and the mechanism chamber with change of pressure of the sample chamber. Note that the pressure of $1x10^{-4}$ corresponds to the gas introduction 10 times as large as the rated maximum gas flow.

Fig. 7. Drift of the stage. The data represent the mean value for 1 min.

Fig. 8. Vibration of the stage. (a) time evolution; (b) power spectrum.

Fig. 9. Drift of the optical column.

Fig. 10. Exposed scale pattern (portion) for measurement of stitching and overlay accuracy. (a) gain bars; (b) rotation verniers; (c) overlay verniers.

Fig. 11. Stitching and overlay accuracy. (a) gain; (b) rotation; (c) overlay.

Fig. 12. SEM image of 60 nm pitch lines delineated onto PMMA resist with the 50 kV EB, where the probe current is 115 pA and the linedose is 0.67 nC/cm. The sample is coated with AuPd for observation.

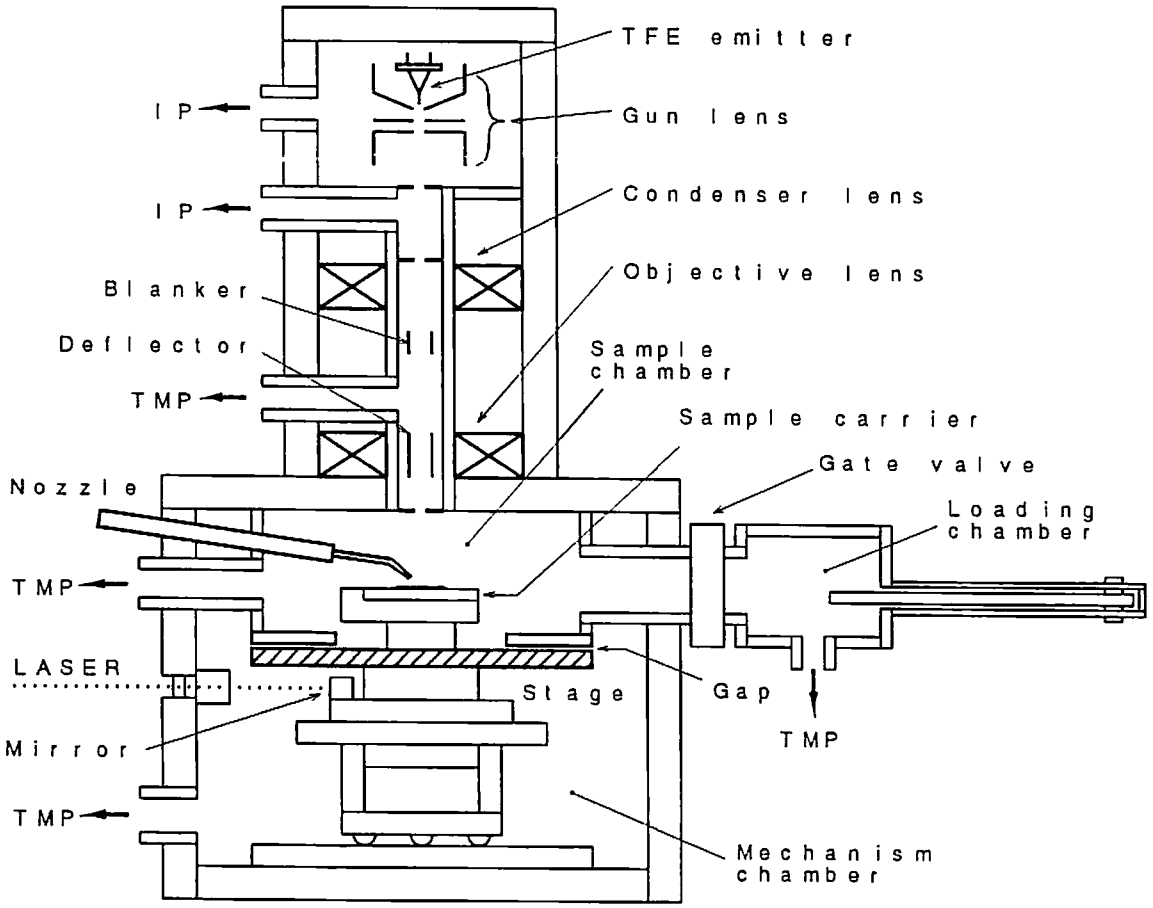

Fig. 1.

H. Hitoshima

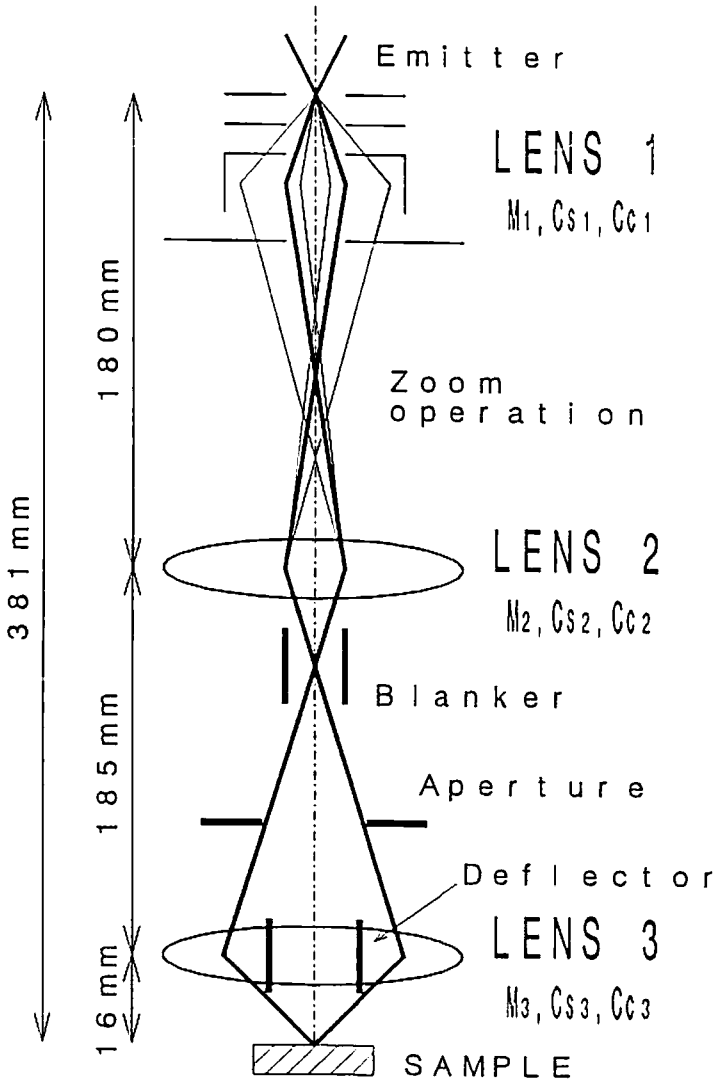

Fig. 2.

H. Hiroshima

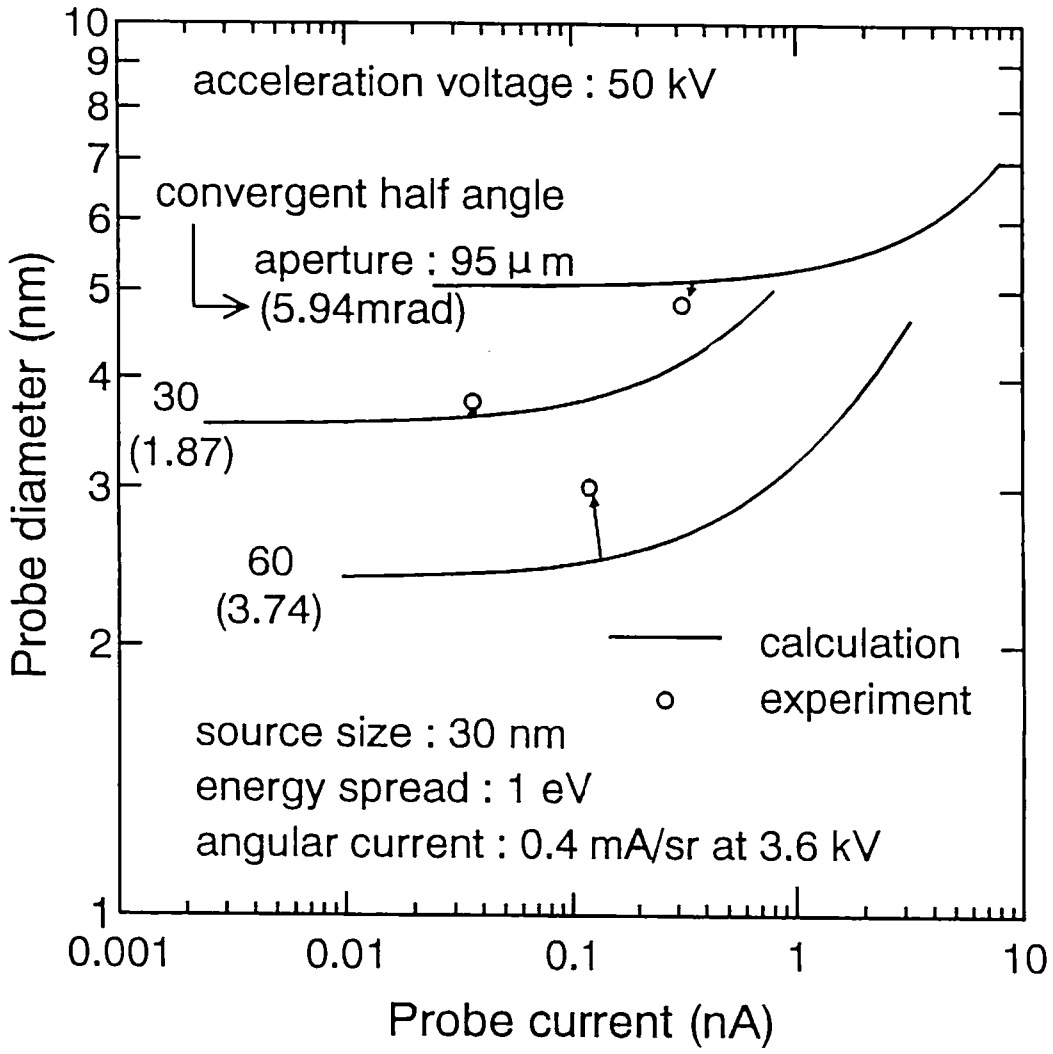

Fig. 3.

H. Hiroshima

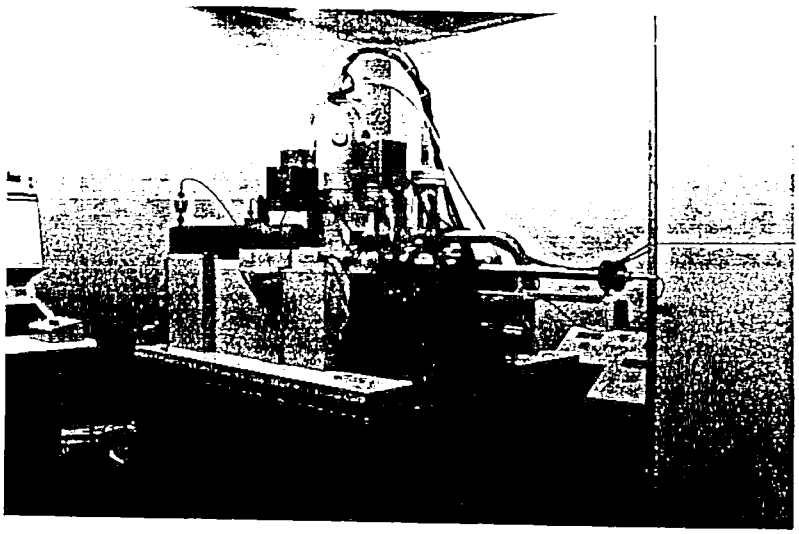

Fig. 4.

(a)

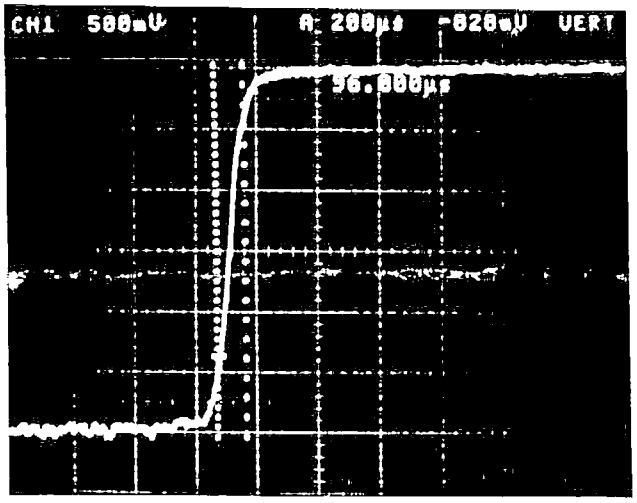

→| |← 3.0 nm

(b)

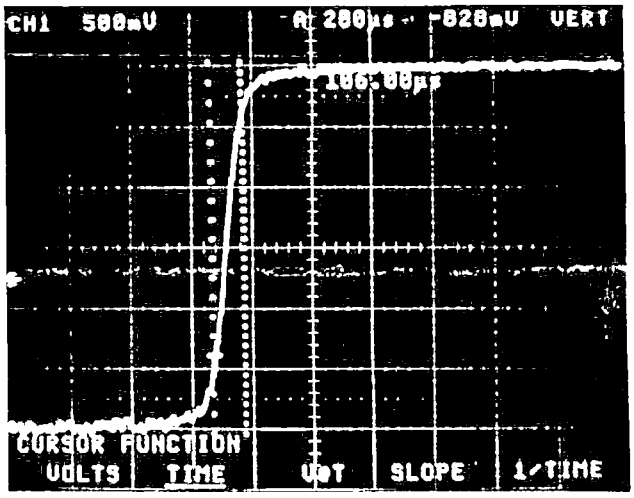

→| |← 3.6 nm

Fig. 5

H. Hiroshima

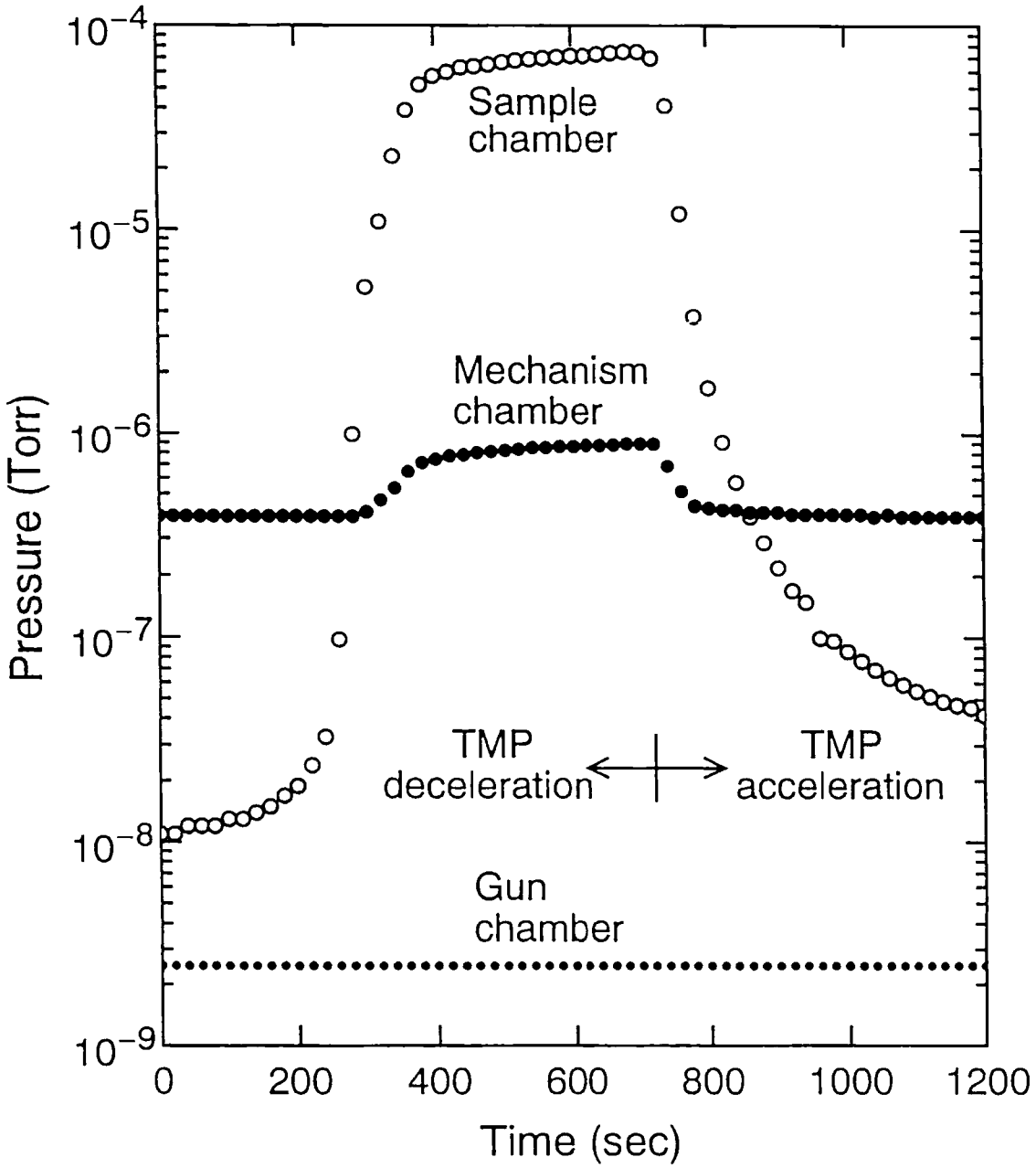

Fig. 6.

H. Hiroshima

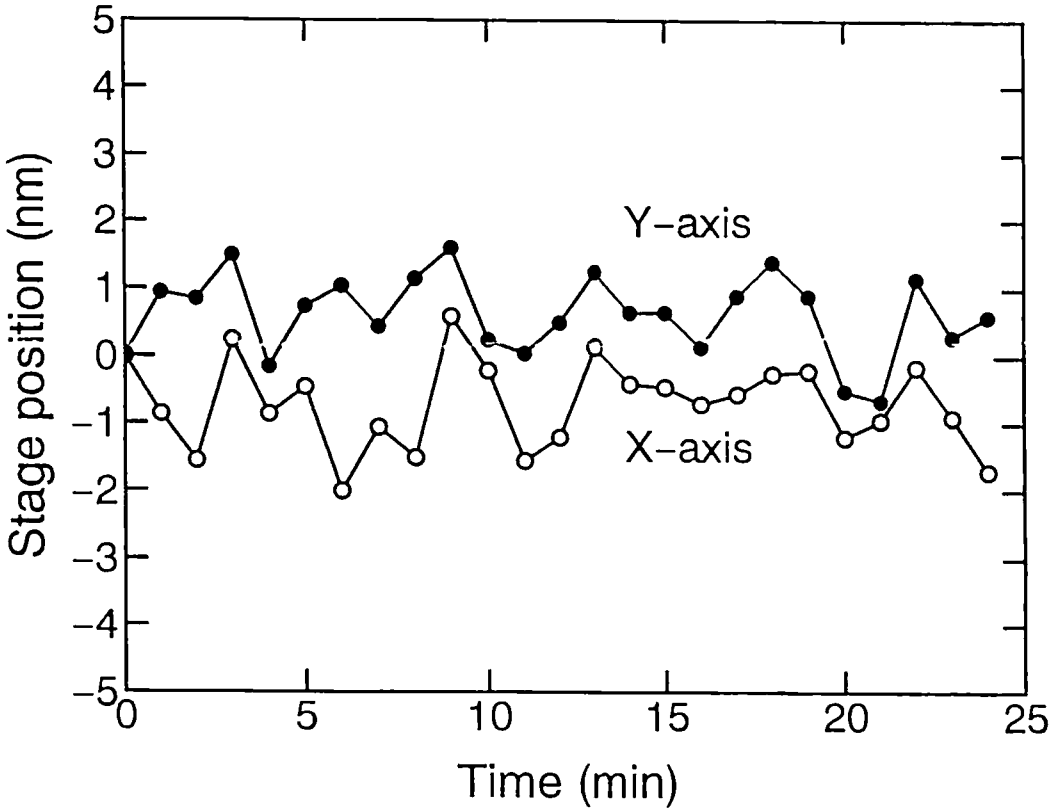

Fig. 7

H. Hiroshima

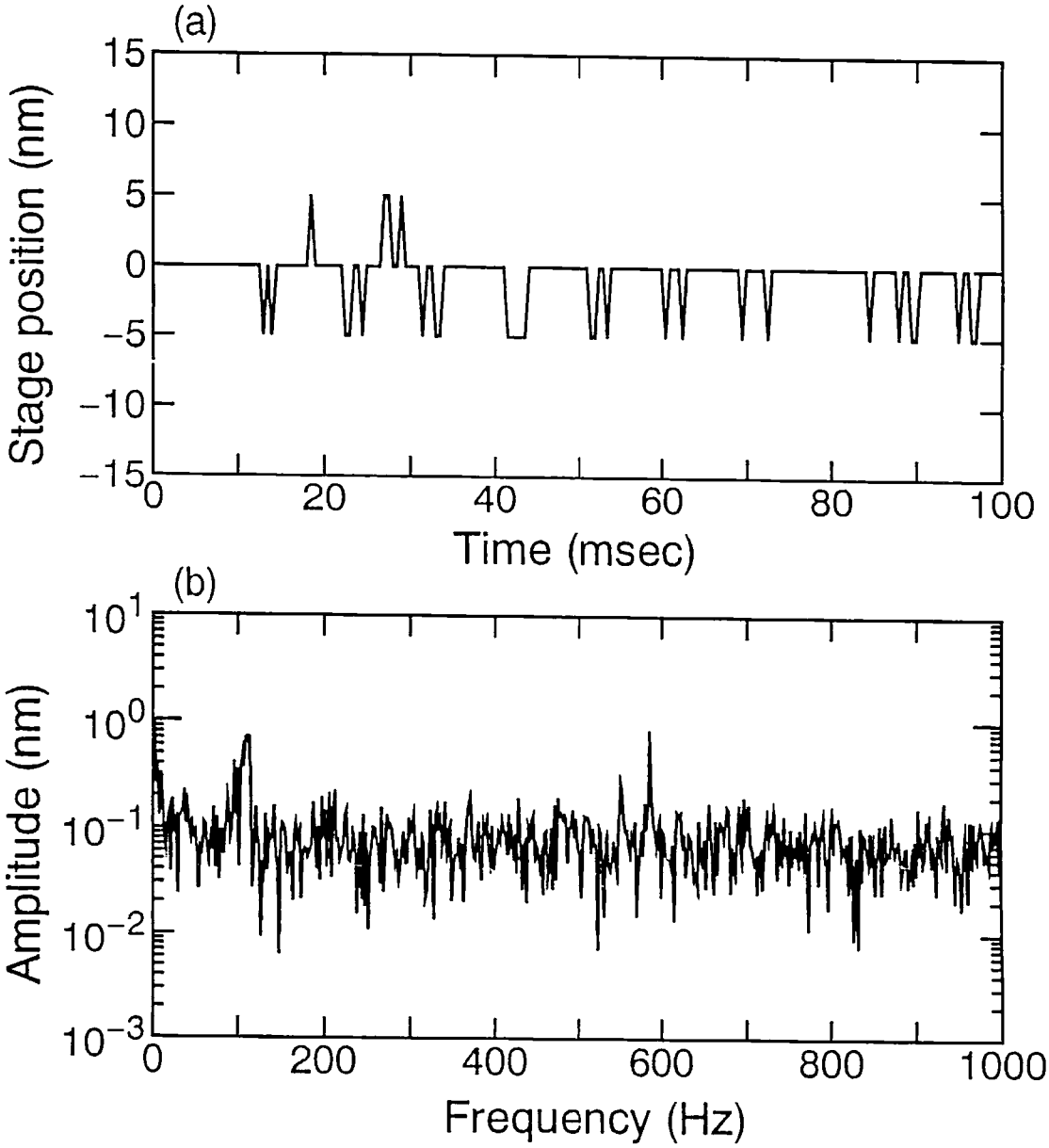

Fig. 8.

H. Hiroshima

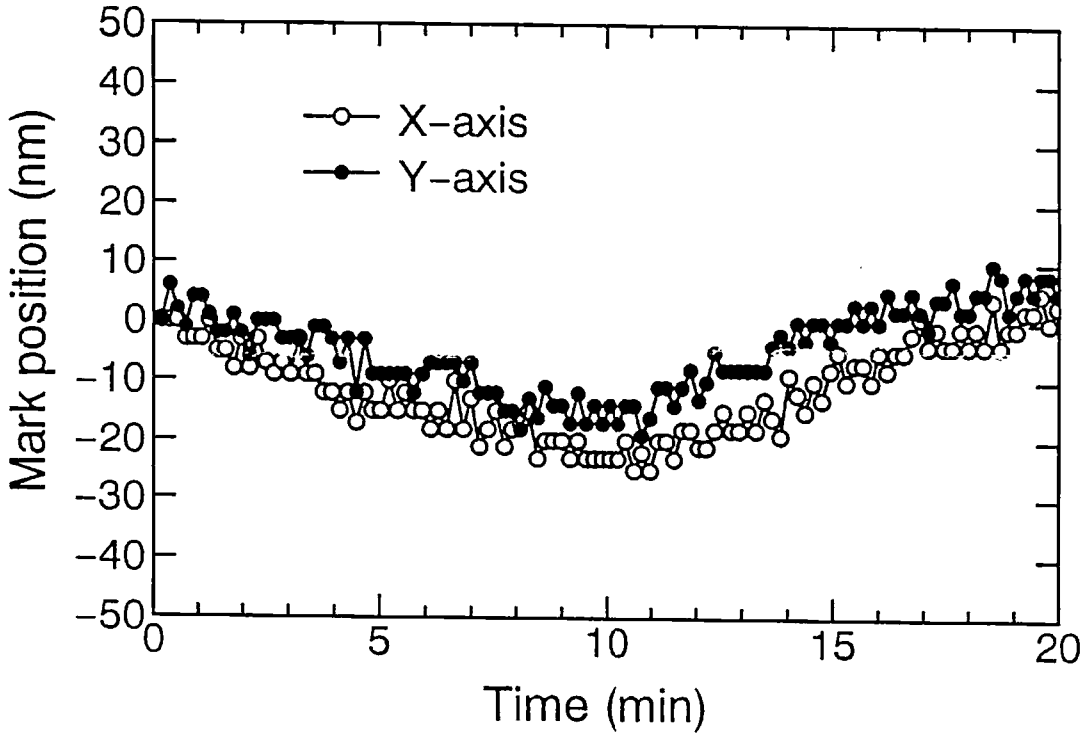

Fig. 9

H. Hiroshima

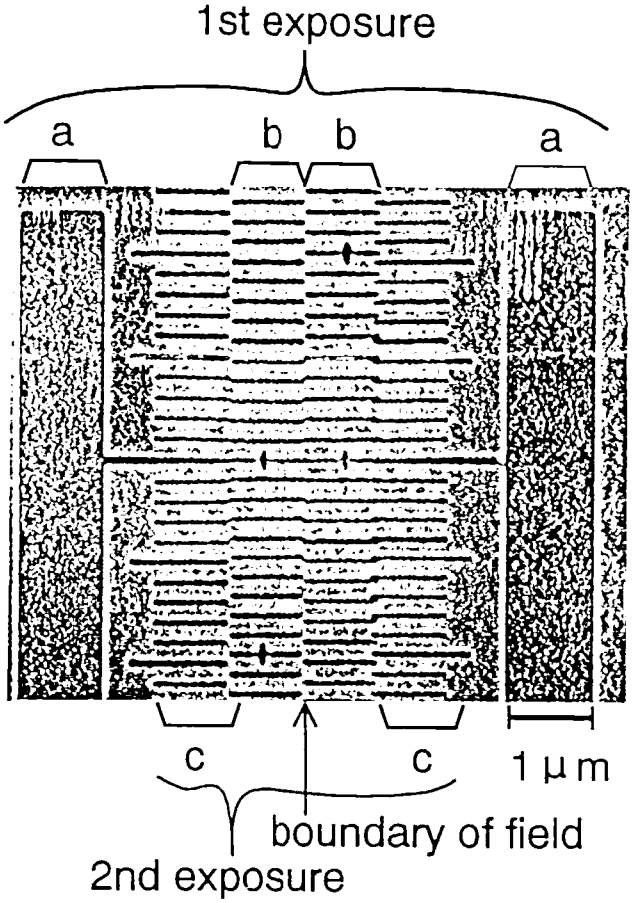

Fig. 10

H. Hiroshima

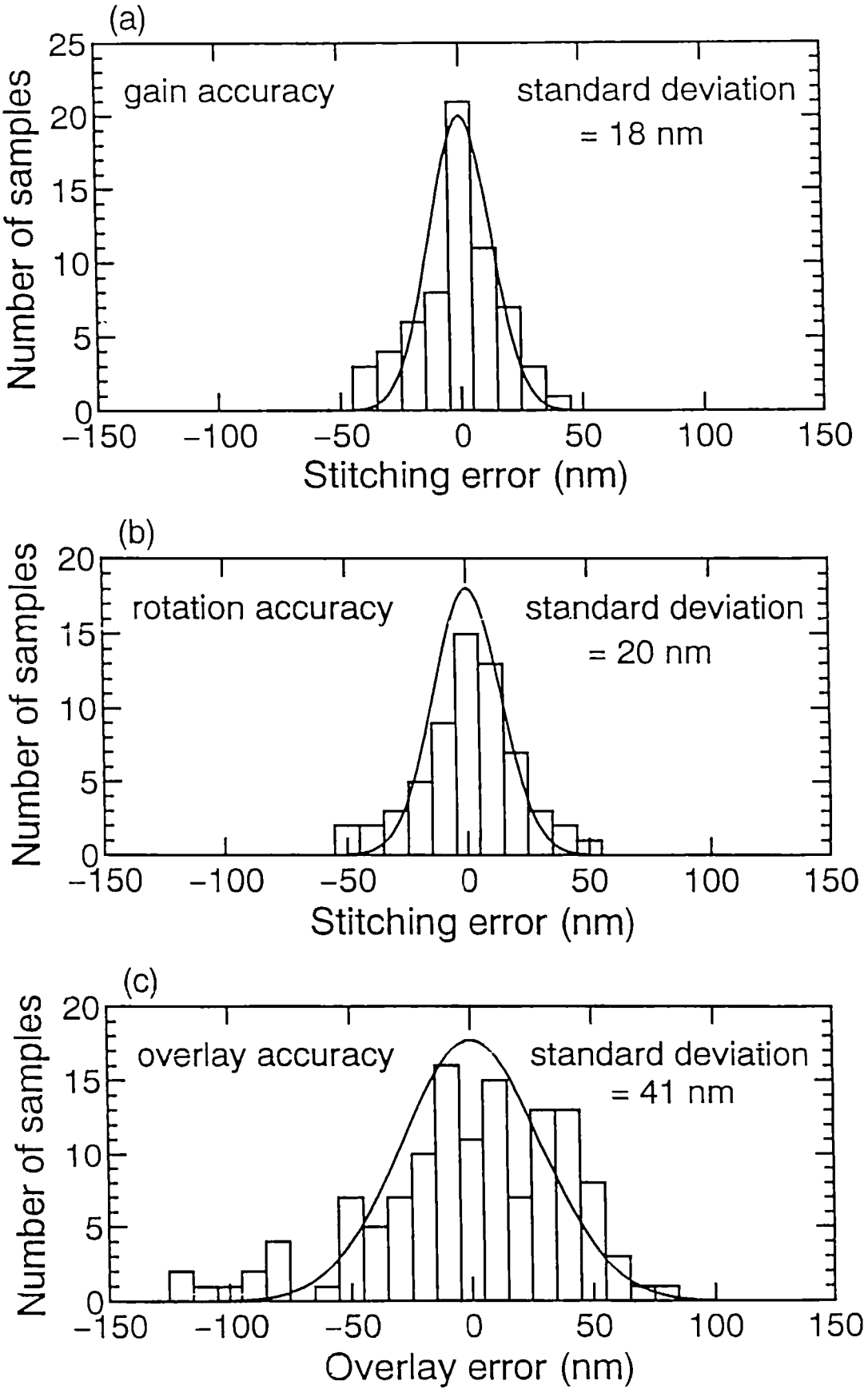

Fig. 11

H. Hiroshima

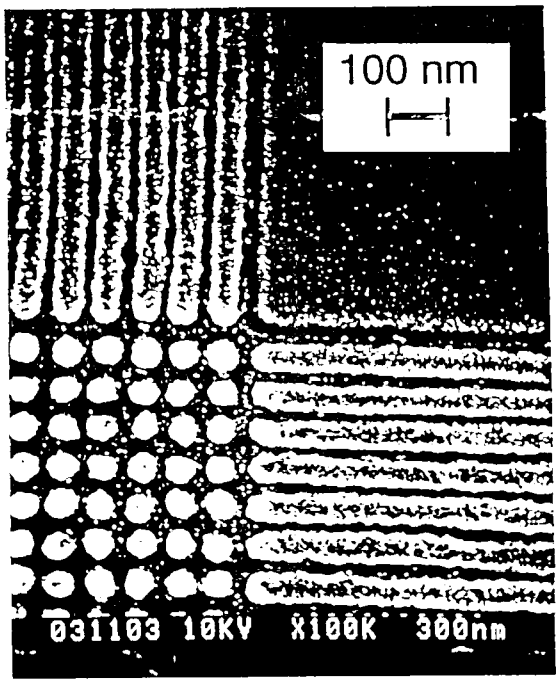

Fig. 12

H. Hiroshima